Geochemical Perspectives Letters

Fluid-melt Mo isotope fractionation: implications for the $\delta^{98/95}$Mo of the upper crust

R. Bezard[1*,‡], H. Guo[2*,‡]

OPEN ACCESS

https://doi.org/10.7185/geochemlet.2320

Abstract

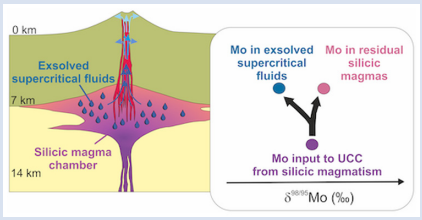

The isotopic composition ($\delta^{98/95}$Mo) of the modern upper continental crust (UCC) remains uncertain. A UCC estimate modelled from the $\delta^{98/95}$Mo of igneous rocks does not converge with constraints derived from the $\delta^{98/95}$Mo of magmatic-hydrothermal molybdenite (MoS_2), a mineral used as a proxy for UCC lithologies. To shed light on this discrepancy, we experimentally determined equilibrium Mo isotope fractionation values between exsolved fluids and melts ($\Delta^{98/95}Mo_{fluid\text{-}melt}$) in shallow felsic magmatic systems. We show that light Mo isotopes are preferentially incorporated in aqueous supercritical fluids in equilibrium with silicic melts, with $\Delta^{98/95}Mo_{fluid\text{-}melt}$ ranging from −0.43 ‰ to −0.17 ‰. The $\delta^{98/95}$Mo of exsolved fluids equilibrated in upper crustal silicic reservoirs should therefore be lighter than co-existing silicic melts. Since felsic plutonic rocks make ~50 % of the UCC, estimates of UCC $\delta^{98/95}$Mo entirely based on igneous rock compositions or based on minerals (MoS_2) growing in magmatic-hydrothermal systems alone will lead to divergent values. Our results can therefore explain the discordance between current UCC $\delta^{98/95}$Mo constraints and provide new ones, representing a key step toward the determination of a robust estimate.

Received 8 March 2023 | Accepted 1 June 2023 | Published 23 June 2023

Introduction

The Mo stable isotopic system is a very promising tool to explore both the chemical evolution of the silicate Earth (*e.g.*, McCoy-West *et al.*, 2019) and the palaeo-redox conditions of oceans (*e.g.*, Wille *et al.*, 2007). Mass balance models associated with both types of applications strongly rely on the Mo isotopic composition ($\delta^{98/95}Mo = 1000 \times [(^{98}Mo/^{95}Mo_{sample})/(^{98}Mo/^{95}Mo_{standard}) - 1]$) of the continental crust (CC), especially its upper layer (UCC), because it is highly enriched in Mo and in direct contact with the hydrosphere. While an estimate for the Mo stable isotope composition of the UCC created prior to the Great Oxidation Event (GOE; ~2.4–2.2 Ga) exists ($\delta^{98/95}Mo = +0.03$ ‰; Greaney *et al.*, 2020), constraints on post-GOE UCC $\delta^{98/95}$Mo are scarce and conflicting. The difficulty in constraining the $\delta^{98/95}$Mo of the UCC after the GOE is a consequence of the redox sensitivity of Mo and its fluid-mobility under oxidising conditions. These properties, for instance, prevent the usage of fine grained clastic sedimentary rocks for that purpose (*e.g.*, Greaney *et al.*, 2020). One approach to constrain the $\delta^{98/95}$Mo of modern UCC has been to use the signatures of molybdenites (MoS_2), mostly derived from magmatic-hydrothermal fluids, as proxies for exposed rocks. It was initially thought that isotopic fractionation would be minor in high temperature systems and that, MoS_2 could therefore represent the isotopic composition of their crustal source rocks (*e.g.*, Barling *et al.*, 2001). As studies multiplied, it became clear that the controls on Mo isotopes in hydrothermal systems were more complex than initially thought (*e.g.*, Hannah *et al.*, 2007). Nevertheless, because these controls were inferred to result in progressively heavier MoS_2, a global average for MoS_2 $\delta^{98/95}$Mo was suggested to represent a maximum value for Phanerozoic UCC (Greber *et al.*, 2014). This, however, is at odds with a recent Phanerozoic UCC composition derived from igneous rock compositions ($\delta^{98/95}Mo = +0.14 \pm 0.07$ ‰; Yang *et al.*, 2017), since the latter is visibly heavier than the most recent MoS_2 $\delta^{98/95}$Mo averages (+0.04 ‰ in Breillat *et al.*, 2016; −0.04 ‰ in Willbold and Elliott, 2017). Clearly, current constraints on Phanerozoic UCC do not converge, and deriving a robust estimate will require a better understanding of magmatic-hydrothermal systems.

One geological process having the potential to create the discrepancy described above is Mo isotopic fractionation during fluid exsolution in silicic systems. The dominant igneous rock types in the UCC are plutonic silicic rocks, and these lithologies were shown to be depleted in Mo (20–90 % depletion; mean 60 %) compared to fluid immobile elements of similar incompatibility (*e.g.*, Ce and Pr; Greaney *et al.*, 2018). In some plutonic suites, correlations between Mo and fluid soluble elements exist, suggesting fluid exsolution as a dominant control over the Mo depletions observed (Greaney *et al.*, 2018). Significant Mo partitioning in magmatic fluids is also supported by a large number of experimental (*e.g.*, Candela and Holland, 1984) and empirical (*e.g.*, Zajacz *et al.*, 2008) studies. Whether isotopic fractionation is associated with this process remains unclear, with only one empirical study suggesting a possible enrichment of heavy Mo isotopes in fluids in a Mo porphyry deposit (Questa, USA; Greber *et al.*, 2014). This is based on the very low Mo and light

1. Department of Geochemistry and Isotope Geology, University of Göttingen, Goldschmidtstrasse 1, 37077 Göttingen, Germany
2. School of Earth Sciences, China University of Geosciences, Wuhan 430074, China
‡ Contributed equally to the manuscript
* Corresponding authors (emails: rachel.bezard@uni-goettingen.de, haihao.guo@cug.edu.cn)

$\delta^{98/95}$Mo of a porphyry rhyolite dike compared to the molybdenites in the nearby and contemporaneous Questa mineralisation. However, the porphyry dike is altered and may not derive from the same magma as that from which the fluids of the mineralisation are derived (Greber *et al.*, 2014 and references therein). Furthermore, theoretical constraints suggest that, in the occurrence of isotopic fractionation, a preferential enrichment of light Mo isotopes in the fluids should occur. This is because Mo coordination in silicate melts is tetrahedral, while both tetrahedral and octahedral coordination have been inferred for Mo in magmatic-hydrothermal fluids (*e.g.*, Borg *et al.*, 2012). Given that most MoS_2 measured thus far have crystallised from fluids exsolved from silicic magmas or melts highly enriched in those fluids (Breillat *et al.*, 2016), a preferential enrichment in light Mo isotopes in the fluids could explain the lighter $\delta^{98/95}$Mo of MoS_2 averages, compared to average silicic rocks ($\delta^{98/95}$Mo = +0.16 ‰ in Yang *et al.*, 2017) and the associated discrepancies in UCC constraints. It is therefore the aim of this contribution to establish the first experimental constraints of the fluid/melt equilibrium fractionation value of Mo stable isotopes ($\Delta^{98/95}Mo_{fluid\text{-}melt} = \delta^{98/95}Mo_{fluid} - \delta^{98/95}Mo_{melt}$) at temperatures, fluid salinities, melt compositions and oxygen fugacities relevant to supercritical fluid exsolution in upper crustal silicic magmatic systems.

Methods

Twelve experiments were conducted at McGill University and Institut des Sciences de la Terre d'Orléans (ISTO) to simulate the equilibration of exsolved fluids with upper crustal felsic magmas. Conditions for each experiment are shown in Table 1. Cold seal pressure vessels were used, except for two experiments (Mo21 and Mo27) requiring the usage of internally heated pressure vessels (IHPV) to allow for higher temperature (900 °C) or higher oxygen fugacity (~FMQ+3). Powders of Mo-doped haplogranitic glasses ($n = 11$) or non-doped natural obsidian ($n = 1$) were loaded into gold capsules together with Mo-free fluids in similar proportions (1:1) (see Supplementary Information for details on the experimental approach). The experiments were equilibrated at 200 MPa, a pressure relevant for most long lived magma chambers (*e.g.*, Huber *et al.*, 2019). At such conditions, a single magmatic fluid phase with low to intermediate salinity (*e.g.*, 1–5 wt. % NaCl in Rusk *et al.*, 2004), a supercritical fluid, exsolves from magmas (Burnham, 1979). We therefore set the range of salinity of our experimental fluids accordingly (0.5–1.5 M (Na,K)Cl). The effects of changing temperature, melt aluminium saturation index (ASI) and oxygen fugacity (fO_2) on $\Delta^{98/95}Mo_{fluid\text{-}melt}$ were also assessed over ranges relevant for upper crustal silicic magma chambers (see Table 1). In similar experiments, chemical equilibrium is typically reached within a maximum of 10 days (*e.g.*, Jiang *et al.*, 2021 and references therein). Time scales for chemical and isotopic equilibrium were therefore assessed *via* a series of identical experiments performed at 800 °C with durations ranging from 1 to 20 days.

Mo isotope compositions and Mo concentrations of starting glasses, final (quenched) glasses and fluids were measured using double spike MC-ICP-MS at the University of Göttingen. The detailed description of the analytical approach is shown in the Supplementary Information. The uncertainty presented for the $\delta^{98/95}$Mo of each sample corresponds to twice the standard deviation of the replicate analyses of the Japan Geological Survey reference materials (±0.05 ‰).

Table 1 Experimental conditions and results.

Experiment ID	Starting material*	T (°C)	Duration (days)	Starting glass ASI	(Na,K)Cl in fluid (mol/L)	fO_2	$\delta^{98/95}Mo_{melt}$ (‰)**	$C_{Mo,melt}$ (µg/g)	$\delta^{98/95}Mo_{fluid}$ (‰)**	$C_{Mo,fluid}$ (µg/g)	$D_{fluid\text{-}melt}$	$\Delta^{98/95}Mo_{fluid\text{-}melt}$ (‰)**
Mo15	HG 1A	700	20	1	1	~FMQ+1	0.12	171	−0.31	47	0.28	−0.43
Mo22	HG 1A	800	1	1	1	~FMQ+1	0.08	197	−0.23	43	0.22	−0.30
Mo02	HG 1A	800	5	1	1	~FMQ+1	0.06	184	−0.25	48	0.26	−0.31
Mo03	HG 1A	800	10	1	1	~FMQ+1	0.09	176	−0.24	56	0.32	−0.32
Mo16	HG 1A	800	10	1	1	~FMQ+1	0.07	188	−0.26	52	0.28	−0.33
Mo07	HG 1A	800	20	1	1	~FMQ+1	0.09	171	−0.26	52	0.30	−0.36
Mo21	HG 1A	900	7	1	1	~FMQ+1	0.11	175	−0.24	59	0.34	−0.35
Mo05	HG 1A	800	10	1	0.5	~FMQ+1	0.07	187	−0.24	51	0.27	−0.32
Mo33	HG 1A	800	11	1	1.5	~FMQ+1	0.05	170	−0.26	63	0.37	−0.31
Mo27	HG 1B	800	10	1	1	~FMQ+3	0.03	269	−0.19	102	0.38	−0.22
Mo08	HG 0.8	800	10	0.80	1	~FMQ+1	0.05	245	−0.13	148	0.60	−0.17
Mo24	Nat. obsi.	800	10	0.85	1.5	~FMQ+1	0.19	5.8	−0.04	2.4	0.40	−0.23

Abbreviations: ASI, aluminum saturation index; fO_2, oxygen fugacity relative to the fayalite-magnetite-quartz buffer (FMQ).
* HG 1A: haplogranite with ASI = 1, 254 µg/g Mo and $\delta^{98/95}$Mo = −0.01 ± 0.05 ‰. HG 1B: haplogranite with ASI = 1, 383 µg/g Mo and $\delta^{98/95}$Mo = −0.01 ± 0.05 ‰. HG 0.8: haplogranite with ASI = 0.8, 421 µg/g Mo and $\delta^{98/95}$Mo = −0.01 ± 0.05 ‰. HG 1A, HG 1B and HG 0.8 contain 78.7 wt. % SiO_2. Nat. obsi.: natural obsidian with ASI = 0.85, 76.7 wt. % SiO_2, 8.8 µg/g Mo and $\delta^{98/95}$Mo = 0.13 ± 0.05 ‰.
** Error on $\delta^{98/95}$Mo is 0.05 ‰; error on $\Delta^{98/95}Mo_{fluid\text{-}melt}$ is propagated (0.07 ‰).

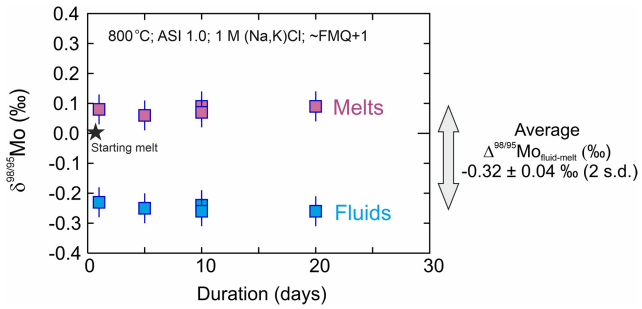

Figure 1 Mo isotopic composition ($\delta^{98/95}$Mo) of fluids and melts *versus* time. All experiments are identical except for their duration (days). Two experiments were performed for the 10 day duration. The average $\Delta^{98/95}Mo_{fluid\text{-}melt}$ (‰) for the 5 experiments is also shown.

Results

$\delta^{98/95}$Mo values and Mo concentrations of starting materials and experimental results are presented in Table 1, together with the calculated Mo partition coefficients between fluid and melt ($D_{fluid\text{-}melt} = C_{Mo,fluid}/C_{Mo,melt}$) and the $\Delta^{98/95}Mo_{fluid\text{-}melt}$ for each pair. The $D_{fluid\text{-}melt}$ and $\Delta^{98/95}Mo_{fluid\text{-}melt}$ of identical experiments produced at different durations (the time series experiments; Figs. 1, 2) suggest that both chemical and isotopic equilibrium were reached between 5 and 10 days at 800 °C. This is consistent with chemical equilibrium time scales observed in similar experimental studies (*e.g.*, Jiang *et al.*, 2021 and references therein). Therefore, with the exception of the 1 and 5 days experiments, all presented experimental data represent equilibrium values.

At equilibrium, $D_{fluid\text{-}melt}$ range from 0.27 to 0.60 and overlap the literature range for similar experiments (*e.g.*, compilation in Fang and Audétat, 2022). $\Delta^{98/95}Mo_{fluid\text{-}melt}$ range from −0.43 ± 0.07 ‰ to −0.17 ± 0.07 ‰ (Fig. 2) and therefore indicate the preferential incorporation of light Mo isotopes in fluids under all investigated conditions, and whether or not the starting glass was doped. The data set shows a clear control of the melt ASI over $\Delta^{98/95}Mo_{fluid\text{-}melt}$ (linear regression with $R^2 = 0.99$; Fig. 3a) with the greatest isotopic differences observed in the samples with the least peralkaline compositions. No effect of fluid salinity is observed (Fig. 3b). Apparent systematics suggest that $\Delta^{98/95}Mo_{fluid\text{-}melt}$ could be larger at lower temperatures and lower oxygen fugacities (Fig. 3c, d), but this is not resolvable in this data set, and further experimental investigation will be required to test these possible correlations.

Interpretation and Discussion of Experimental Results

The experimental data suggest that silicic melts with geologically realistic ASI will preferentially lose light Mo isotopes to exsolved supercritical fluids. In theory, both a difference in coordination and valence state of Mo between fluid and melt could induce the isotopic fractionation observed, *i.e.* higher coordination and/or lower valence state of Mo in the fluid than in the melt (*e.g.*, Urey, 1947). However, thermodynamic and empirical evidence suggests that the valence state of Mo should be similar in silicate melts and associated magmatic-hydrothermal fluids, *i.e.* hexavalent (*e.g.*, Kaufmann *et al.*, 2021; Willbold and Elliott, 2017 and references therein). Therefore, the most likely driver behind the $\Delta^{98/95}Mo_{fluid\text{-}melt}$ observed in our experiments is higher Mo coordination in the fluid compared to the melt. In silicate melts, Mo dominantly occurs as tetrahedral molybdate species (MoO_4^{2-}). On the other hand, in high temperature fluids, the coordination of Mo remains debated. Some studies suggested that Mo dominantly occurs as Na-K molybdate, monochloride or thiomolybdate at modest salinity, and as Mo-oxy-hydroxy complexes at low salinity (Zhang *et al.*, 2012; Tattitch and Blundy, 2017). In such cases, Mo would be tetrahedrally coordinated, and no isotopic fractionation should be observed between fluids and melts, which is inconsistent with our experimental results. However, others have suggested the occurrence of species involving octahedrally coordinated Mo. For instance, Ulrich and Mavrogenes (2008) suggested the presence of a chloro-oxo Mo (VI) complex in high salinity (>20 % KCl) fluids (at 490 °C and ≥150 MPa). Borg *et al.* (2012), based on experiments performed at lower temperatures and pressures (up to 385 °C, 60 MPa), found that octahedral species were becoming predominant in increasingly acidic solutions (pH < 5), with species such as molybdic acid and chloro-oxo Mo complexes. They also showed that increasing temperature favoured the formation of oxo-chloro complexes and suggested that these could be responsible for Mo transport in less acidic solutions at higher temperature (*e.g.*, 700 °C), as proposed by Ulrich and Mavrogenes (2008). Based on the lack of correlation between $\Delta^{98/95}Mo_{fluid\text{-}melt}$ and starting fluid salinity in our experiments, a control of Mo isotopes by chloro-oxo Mo complexes alone seems unlikely. Hence, at least one other species in which Mo coordination is greater than tetrahedral, perhaps molybdic acid, is required in

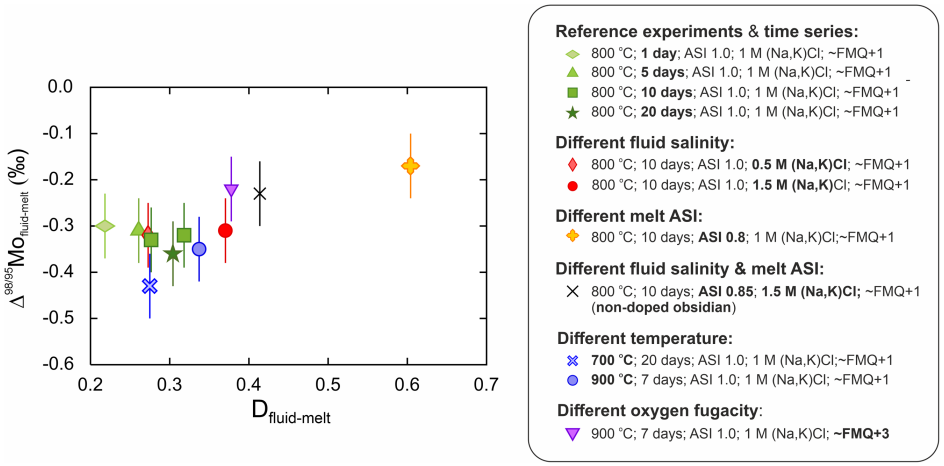

Figure 2 Mo isotope fractionation value between fluid and melt ($\Delta^{98/95}Mo_{fluid\text{-}melt}$) *versus* the partition coefficient ($D_{fluid\text{-}melt} = C_{fluid}/C_{melt}$) for each experiment.

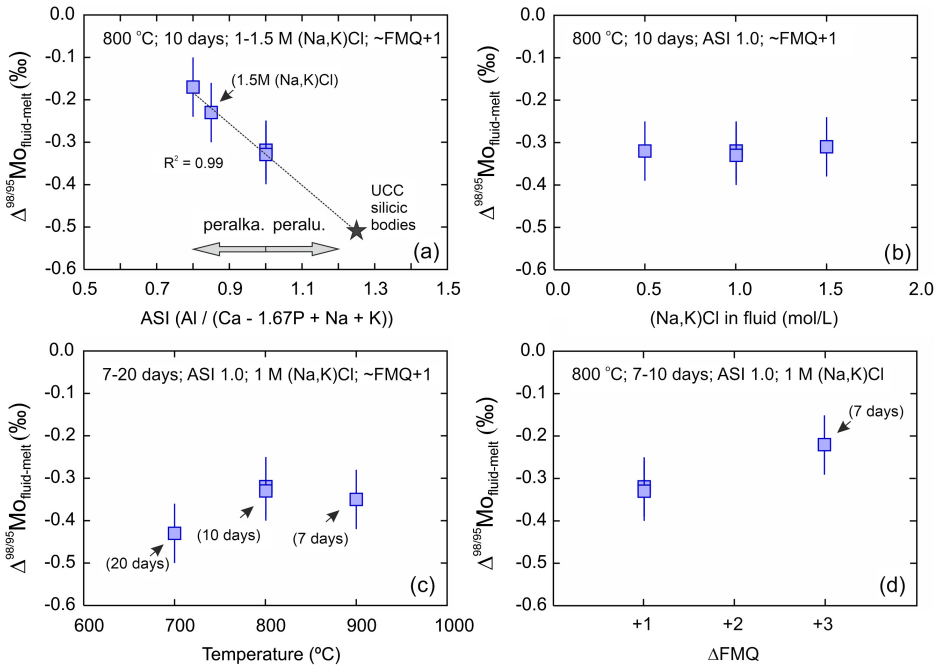

Figure 3 Evolution of the Mo isotope fractionation value between fluids and melts ($\Delta^{98/95}Mo_{fluid\text{-}melt}$) at different experimental **(a)** melt aluminium saturation indexes (ASI = Al/(Ca – 1.67P + Na + K)), **(b)** fluid salinities, **(c)** temperatures and **(d)** oxygen fugacities (fO_2 relative to the fayalite-magnetite-quartz buffer, FMQ). Abbreviations: peralka., peralkaline; peralu., peraluminous.

the fluids to explain the systematics observed in our experiments. Finally, the negative correlation between $\Delta^{98/95}Mo_{fluid\text{-}melt}$ and ASI suggests that the latter exerts a strong influence on the coordination of Mo.

Implications for the Composition of the Upper Continental Crust

Most large and long lived silicic magma chambers are located at upper crustal levels corresponding to lithostatic pressures of ~200 MPa (Huber *et al.*, 2019). There, significant amounts of exsolved supercritical fluids accumulate and equilibrate with silicic magmas. Slow fluid exsolution associated with the cooling and crystallisation of the melt is punctuated by repetitive fast exsolution events associated with decompression of incoming recharging melt (*e.g.*, Edmonds and Woods, 2018). Our data indicate that the extraction of these exsolved fluids likely results in the removal of light Mo from magma bodies, including precursor bodies of the silicic plutonic rocks making ~50 % of the UCC (*e.g.*, Wedepohl, 1995). The Mo depletion of these plutons (*e.g.*, Greaney *et al.*, 2018), together with the large number of experimental constraints, suggests that a significant Mo fraction must have been removed from their precursor melts *via* exsolved fluids. Since UCC silicic plutonic rocks are dominantly peraluminous (ASI ≈ 1.25; Wedepohl, 1995), our experiments suggest that resolvable $\Delta^{98/95}Mo_{fluid\text{-}melt}$ likely applied during the devolatilisation of their precursor melt. In other words, the $\delta^{98/95}Mo$ of UCC silicic plutons should be heavier than their precursor, undegassed melts. Based on our $D_{fluid\text{-}melt}$, the difference between undegassed and degassed silicic magmas might, however, not be large. For instance, using the highest $D_{fluid\text{-}melt}$ in our experiments and assuming an extreme scenario whereby a hydrous melt with 10 wt. % volatiles undergoes fluid exsolution with a $\Delta^{98/95}Mo_{fluid\text{-}melt}$ of −0.51 ‰ (extrapolation of the linear regression to ASI = 1.25 in Fig. 3a), would result in a residual melt that is only 0.03 ‰ heavier than the undegassed melt (see Supplementary Information for calculation). This is smaller than our analytical uncertainty. However, the range of published $D_{fluid\text{-}melt}$ for similar experiments is large and includes significantly higher values (*e.g.*, compilation in Fang and Audétat, 2022). It is therefore best to consider the average $\delta^{98/95}Mo$ of UCC silicic plutonic rocks (Yang *et al.*, 2017) as a maximum value for the signature of the total Mo contribution to the UCC from undegassed silicic magmatism. In turn, UCC $\delta^{98/95}Mo$ estimates derived from igneous rocks should also be viewed as maxima.

Based on our experiments, the average $\delta^{98/95}Mo$ of UCC silicic rocks should also be clearly heavier than global $\delta^{98/95}Mo$ average for UCC MoS_2, since MoS_2 measured thus far are from magmatic-hydrothermal systems. There, MoS_2 crystallises from both brines and low salinity vapours that unmix from supercritical fluids once they reach a miscibility gap in the NaCl-H_2O system during ascent in the shallowest part of magmatic-hydrothermal complexes (typically <140 MPa and 400–700 °C; *e.g.*, Bodnar *et al.*, 1985). The average UCC silicic rock composition ($\delta^{98/95}Mo = +0.16$ ‰) of Yang *et al.* (2017) is indeed ~0.18 ‰ and ~0.12 ‰ heavier than the two most extensive and recent MoS_2 global averages of Willbold and Elliott (2017) and Breillat *et al.* (2016) (−0.04 ‰ and +0.04 ‰, respectively), in agreement with the direction of isotopic fractionation in the experiments. The isotopic difference between UCC silicic rocks and UCC magmatic-hydrothermal MoS_2 averages is however smaller than suggested by the experimental $\Delta^{98/95}Mo_{fluid\text{-}melt}$ values. In the experiments, equilibrated melts are up to 0.4 ‰ heavier than associated supercritical fluids, and while this will need to be confirmed in future experiments, the negative correlation between $\Delta^{98/95}Mo_{fluid\text{-}melt}$ and ASI suggests that even greater values could apply during exsolution from more peraluminous melts, such as those of the plutons dominating the UCC. While other factors are possible, this smaller isotopic difference could simply be the consequence of the timing of fluid exsolution relative to mineral fractionation in silicic magma chambers. Most recent studies suggest that long lived silicic magma reservoirs are largely crystallised between recharge events (*e.g.*, Schmitt *et al.*, 2010). Hence, over the lifespan of a silicic magma body, most exsolved fluids will

equilibrate with interstitial melts of crystal mushes. These interstitial melts are expected to be enriched in Mo, since it is an incompatible element. More importantly, based on the Mo coordination (octahedral) in all minerals capable of carrying significant amount of Mo in the mush (Ti-bearing oxides, biotite, amphibole, K feldspar; Greaney *et al.*, 2018), interstitial melts (in which Mo is tetrahedral) are most likely isotopically heavier than the bulk mush. Exsolved fluids in equilibrium with these melts should therefore be heavier than hypothetical fluids in equilibrium with bulk mushes or fully crystallised equivalents. This would explain the smaller isotopic difference between UCC silicic rocks and UCC MoS_2 averages, than expected based on the experiments herein.

Overall, our results provide a solution for the discrepancy between the UCC $\delta^{98/95}$Mo estimate derived from exposed igneous UCC rocks and constraints obtained from average UCC MoS_2. They also stress the lack of straight forward assessment of the UCC $\delta^{98/95}$Mo *via* MoS_2 and suggest that UCC $\delta^{98/95}$Mo derived from igneous rock compositions should be considered as a maximum value.

Acknowledgements

We thank Horst Marschall for the editorial handling of the manuscript and Alex McCoy-West and an anonymous reviewer for constructive reviews. This work was supported by the German Research Foundation grants BE 6670/1-1 and BE 6670/2-1 (RB) and Fundamental Research Funds for the Central Universities, China University of Geosciences (Wuhan) CUG230610 (HG).

Editor: Horst R. Marschall

Additional Information

Supplementary Information accompanies this letter at https://www.geochemicalperspectivesletters.org/article2320.

Cite this letter as: Bezard, R., Guo, H. (2023) Fluid-melt Mo isotope fractionation: implications for the $\delta^{98/95}$Mo of the upper crust. *Geochem. Persp. Let.* 26, 25–30. https://doi.org/10.7185/geochemlet.2320

References

Barling, J., Arnold, G.L., Anbar, A.D. (2001) Natural mass-dependent variations in the isotopic composition of molybdenum. *Earth and Planetary Science Letters* 193, 447–457. https://doi.org/10.1016/S0012-821X(01)00514-3

Bodnar, R.J., Burnham, C.W., Sterner, S.M. (1985) Synthetic fluid inclusions in natural quartz. III. Determination of phase equilibrium properties in the system H_2O-NaCl to 1000°C and 1500 bars. *Geochimica et Cosmochimica Acta* 49, 1861–1873. https://doi.org/10.1016/0016-7037(85)90081-X

Borg, S., Liu, W., Etschmann, B., Tian, Y., Brugger, J. (2012) An XAS study of molybdenum speciation in hydrothermal chloride solutions from 25–385 °C and 600 bar. *Geochimica et Cosmochimica Acta* 92, 292–307. https://doi.org/10.1016/j.gca.2012.06.001

Breillat, N., Guerrot, C., Marcoux, E., Négrel, Ph. (2016) A new global database of δ^{98}Mo in molybdenites: A literature review and new data. *Journal of Geochemical Exploration* 161, 1–15. https://doi.org/10.1016/j.gexplo.2015.07.019

Burnham, C.W. (1979) Magmas and hydrothermal fluids. In: Barnes, H.L. (Ed.) *Geochemistry of Hydrothermal Ore Deposits*. Second Edition, Wiley, New York, 71–136.

Candela, P.A., Holland, H.D. (1984) The partitioning of copper and molybdenum between silicate melts and aqueous fluids. *Geochimica et Cosmochimica Acta* 48, 373–380. https://doi.org/10.1016/0016-7037(84)90257-6

Edmonds, M., Woods, A.W. (2018) Exsolved volatiles in magma reservoirs. *Journal of Volcanology and Geothermal Research* 368, 13–30. https://doi.org/10.1016/j.jvolgeores.2018.10.018

Fang, J., Audétat, A. (2022) The effects of pressure, fO_2, fS_2 and melt composition on the fluid–melt partitioning of Mo: Implications for the Mo-mineralization potential of upper crustal granitic magmas. *Geochimica et Cosmochimica Acta* 336, 1–14. https://doi.org/10.1016/j.gca.2022.08.016

Greaney, A.T., Rudnick, R.L., Gaschnig, R.M., Whalen, J.B., Luais, B., Clemens, J.D. (2018) Geochemistry of molybdenum in the continental crust. *Geochimica et Cosmochimica Acta* 238, 36–54. https://doi.org/10.1016/j.gca.2018.06.039

Greaney, A.T., Rudnick, R.L., Romaniello, S.J., Johnson, A.C., Gaschnig, R.M., Anbar, A.D. (2020) Molybdenum isotope fractionation in glacial diamictites tracks the onset of oxidative weathering of the continental crust. *Earth and Planetary Science Letters* 534, 116083. https://doi.org/10.1016/j.epsl.2020.116083

Greber, N.D., Pettke, T., Nägler, T.F. (2014) Magmatic–hydrothermal molybdenum isotope fractionation and its relevance to the igneous crustal signature. *Lithos* 190–191, 104–110. https://doi.org/10.1016/j.lithos.2013.11.006

Hannah, J.L., Stein, H.J., Wieser, M.E., de Laeter, J.R., Varner, M.D. (2007) Molybdenum isotope variations in molybdenite: Vapor transport and Rayleigh fractionation of Mo. *Geology* 35, 703–706. https://doi.org/10.1130/G23538A.1

Huber, C., Townsend, M., Degruyter, W., Bachmann, O. (2019) Optimal depth of subvolcanic magma chamber growth controlled by volatiles and crust rheology. *Nature Geoscience* 12, 762–768. https://doi.org/10.1038/s41561-019-0415-6

Jiang, Z., Shang, L., Guo, H., Wang, X.-s., Chen, C., Zhou, Y. (2021) An experimental investigation into the partition of Mo between aqueous fluids and felsic melts: Implications for the genesis of porphyry Mo ore deposits. *Ore Geology Reviews* 134, 104144. https://doi.org/10.1016/j.oregeorev.2021.104144

Kaufmann, A.K.C., Pettke, T., Wille, M. (2021) Molybdenum isotope fractionation at upper-crustal magmatic-hydrothermal conditions. *Chemical Geology* 578, 120319. https://doi.org/10.1016/j.chemgeo.2021.120319

McCoy-West, A.J., Chowdhury, P., Burton, K.W., Sossi, P., Nowell, G.M., Fitton, J.G., Kerr, A.C., Cawood, P.A., Williams, H.M. (2019) Extensive crustal extraction in Earth's early history inferred from molybdenum isotopes. *Nature Geoscience* 12, 946–951. https://doi.org/10.1038/s41561-019-0451-2

Rusk, B.G., Reed, M.H., Dilles, J.H., Klemm, L.M., Heinrich, C.A. (2004) Compositions of magmatic hydrothermal fluids determined by LA-ICP-MS of fluid inclusions from the porphyry copper–molybdenum deposit at Butte, MT. *Chemical Geology* 210, 173–199. https://doi.org/10.1016/j.chemgeo.2004.06.011

Schmitt, A.K., Stockli, D.F., Lindsay, J.M., Robertson, R., Lovera, O.M., Kislitsyn, R. (2010) Episodic growth and homogenization of plutonic roots in arc volcanoes from combined U–Th and (U–Th)/He zircon dating. *Earth and Planetary Science Letters* 295, 91–103. https://doi.org/10.1016/j.epsl.2010.03.028

Tattitch, B.C., Blundy, J.D. (2017) Cu-Mo partitioning between felsic melts and saline-aqueous fluids as a function of X_{NaCleq}, f_{O_2}, and f_{S_2}. *American Mineralogist* 102, 1987–2006. https://doi.org/10.2138/am-2017-5998

Ulrich, T., Mavrogenes, J. (2008) An experimental study of the solubility of molybdenum in H_2O and KCl–H_2O solutions from 500 °C to 800 °C, and 150 to 300 MPa. *Geochimica et Cosmochimica Acta* 72, 2316–2330. https://doi.org/10.1016/j.gca.2008.02.014

Urey, H.C. (1947) The Thermodynamic Properties of Isotopic Substances. *Journal of the Chemical Society (Resumed)* 1947, 562–581. https://doi.org/10.1039/jr9470000562

Wedepohl, K.H. (1995) The composition of the continental crust. *Geochimica et Cosmochimica Acta* 59, 1217–1232. https://doi.org/10.1016/0016-7037(95)00038-2

Willbold, M., Elliott, T. (2017) Molybdenum isotope variations in magmatic rocks. *Chemical Geology* 449, 253–268. https://doi.org/10.1016/j.chemgeo.2016.12.011

Wille, M., Kramers, J.D., Nägler, T.F., Beukes, N.J., Schröder, S., Meisel, Th., Lacassie, J.P., Voegelin, A.R. (2007) Evidence for a gradual rise of oxygen between 2.6 and 2.5 Ga from Mo isotopes and Re-PGE signatures in shales. *Geochimica et Cosmochimica Acta* 71, 2417–2435. https://doi.org/10.1016/j.gca.2007.02.019

Yang, J., Barling, J., Siebert, C., Fietzke, J., Stephens, E., Halliday, A.N. (2017) The molybdenum isotopic compositions of I-, S- and A-type granitic suites. *Geochimica et Cosmochimica Acta* 205, 168–186. https://doi.org/10.1016/j.gca.2017.01.027

Zajacz, Z., Halter, W.E., Pettke, T., Guillong, M. (2008) Determination of fluid/melt partition coefficients by LA-ICPMS analysis of co-existing fluid and silicate melt inclusions: Controls on element partitioning. *Geochimica et Cosmochimica Acta* 72, 2169–2197. https://doi.org/10.1016/j.gca.2008.01.034

Zhang, L., Audétat, A., Dolejš, D. (2012) Solubility of molybdenite (MoS_2) in aqueous fluids at 600–800 °C, 200 MPa: A synthetic fluid inclusion study. *Geochimica et Cosmochimica Acta* 77, 175–185. https://doi.org/10.1016/j.gca.2011.11.015

Geochemical Perspectives Letters

Fluid-melt Mo isotope fractionation: implications for the $\delta^{98/95}$Mo of the upper crust

R. Bezard, H. Guo

Supplementary Information

The Supplementary Information includes:

- Experimental and Analytical Methods
- Details for Modelled Impact of Fluid Exsolution in Discussion
- Supplementary Table S-1
- Supplementary Information References

Experimental and Analytical Methods

Preparation of starting materials

The haplogranitic glasses used in the experiments were synthesised from SiO_2, $Al(OH)_3$, Na_2CO_3 and K_2CO_3 (analytical grade). The different alumina saturation indices (ASI = 0.8 and 1) were obtained by changing the abundances of $Al(OH)_3$, Na_2CO_3, and K_2CO_3, while keeping a constant Na/K ratio. In order to dehydrate and decarbonate them, the mixtures were loaded into Pt crucibles, heated in a muffle furnace from 21 °C to 1100 °C (100 °C/h) and kept at 1100 °C for 12 h. After cooling, the mixtures were finely ground in an agate mortar to achieve homogenisation and removal of gas bubbles. They were then doped with ~200–300 µg/g Mo in the form of MoO_3, heated at 1600 °C for 2 h (in a Pt crucible) and the resulting melts were quenched using distilled H_2O. Finally, the glasses were ground to fine powder and melted a last time at 1600 °C for another 2 h (in Pt crucibles) for homogeneity.

The fluids were prepared using deionised H_2O and analytical grade NaCl and KCl to reach (Na,K)Cl with a molar Na to K ratio of 1:1 and concentrations of 0.5, 1 and 1.5 mol/L (M).

High temperature and pressure experiments

The cold-seal pressure vessel (CSPV) experiments were conducted both at McGill University (Canada) and the Institut des Sciences de la Terre d'Orléans (ISTO, France), while the internally heated pressure vessel experiments (IHPV) were performed at ISTO only.

The rapid-quench CSPVs are made of nickel-based superalloy using water as the pressure medium, with a setup similar to that described in Matthews *et al*. (2003). For the IHPV experiments, the samples were pressurised using pure Ar or Ar-H_2 (0.15–0.6 MPa H_2 total pressure) in order to vary fO_2 conditions. The redox conditions used in this study are the apparent oxygen fugacity assuming a water fugacity of 1 for the system. For CSPV experiments, oxygen fugacity was not controlled in the vessels, but should be ~FMQ+1, as indicated by the reaction of water with the autoclave material (Keppler, 2010). For the IHPV experiments (Mo21 and Mo27), oxygen fugacity was controlled using mixtures of Ar and H_2, as mentioned above. The pressure was monitored by a transducer calibrated against a Heise Bourdon gauge with an accuracy of ±2 MPa (Gaillard *et al*., 2001; Andújar *et al*., 2013). The experiments were performed in double-coiled Kanthal with near-isothermal conditions (thermal gradient < 2–3 °C/cm) in the 3 cm long hotspot (Andújar *et al*., 2013). Temperature was controlled using NiCr–Ni (K-type) thermocouples for CSPV and Pt-Pt_{90}-Rh_{10} (S-type) thermocouples for IHPV experiments.

For all experiments, ~0.1 g of glass powder was loaded with a similar amount of aqueous fluid (~0.1 g) into Au capsules with 5.0 mm or 5.4 mm outer diameter, 0.2 mm wall thickness and ca. 2.0 cm length. After welding, capsules were put in an oven at 120 °C to check for potential leaks, and faulty capsules were discarded. The sealed capsules were then loaded into the CSPV or IHPV. Experiments were run at 700–900 °C and 200 MPa for 1–20 days (Table 1) and then quenched by dropping into a cold zone within a few seconds. Variable durations for otherwise identical experiments allowed the assessment of the timing of chemical and isotopic equilibrium at 800 °C, which was achieved between 5 and 10 days. Based on this, the duration was set to 20 days for 700 °C and 7 days for 900 °C experiments (*e.g*., Guo *et al*., 2020a). Capsules were weighted before and after experiments, to identify any obvious weight loss.

Fluid and melt extraction from experimental capsules and preparation

Capsules having preserved their initial weight were cleaned in dilute HCl, followed by at least three rinses with de-ionised H_2O. They were then cooled by liquid N_2 and punctured carefully with a needle prior to fluid extraction using a pipette. The capsule interiors were rinsed with hot and cold deionised water several times in a similar way to that described by Keppler and Wyllie (1991). This is to ensure full dissolution of potentially precipitated material during quenching. The recovered fluids and capsule rinses were transferred into 15 mL pre-cleaned Teflon beakers. The glasses and capsules were dried at 130 °C in the oven for at least 2 h and were weighted to determine the post-quenching fluid weight by subtraction. This approach was shown to be successful in other stable isotope studies (Guo *et al*., 2020a, 2020b, 2021).

Glasses were crushed to fine particles in agate mortars in order to open fluid inclusions that were possibly trapped in the glass. The powders were then transferred to centrifuge tubes and were agitated and centrifuged in Milli-Q H_2O (MQ H_2O; 18.2 MΩ cm). The supernatant (MQ H_2O) was then discarded to release possible contamination from fluid inclusions. The rinsing process was repeated twice more. The powders were then dried in the oven at 60 °C for 24 h.

Digestion and preparation of stock solutions for fluids and melts

For each experiment, between 10 and 20 mg of glass powder was digested in Teflon beakers using twice distilled (2TD; using Savillex DST-1000 distillation units) 14 M HNO_3 and 29 M HF for 72 h at 140 °C. The solutions were then dried down, followed by sample re-dissolution in 14 M HNO_3. The last two steps were repeated again, this time with aqua-regia and 6 M HCl to ensure complete fluoride dissolution. Samples were then equilibrated in 0.5 M HNO_3. Fluids recovered from the capsule and capsule rinses were dried down. They were subsequently handled like the glass samples and all fluids and glasses were equilibrated in 0.5 M HNO_3.

Mo separation and measurement

For each fluid and glass, an aliquot from the stock was spiked with a ^{97}Mo-^{100}Mo mixture and equilibrated in 14 M HNO_3 at 110 °C. The solutions were then dried dry down and the solids were converted into chloride form using 6 M

HCl and then equilibrated in 3 M HCl for Mo separation. The procedure described in Willbold *et al*. (2016) was used to extract Mo from the sample matrix using a single-stage anion (AG1*8 100–200 mesh) column chemistry. After separation, organic matter introduced during chemistry was removed by passing the collected solution through ~200 µL Eichrom prefilter (100–150 µm; PF-B200-A) or by treating the dried down residues with $HClO_4$ (~50 µL) and 14 M HNO_3 (~500 µL). After this, the Mo cut was equilibrated and re-dissolved in 0.4 M HNO_3-0.05 M HF for mass spectrometric analysis.

The samples were measured using the ThermoScientific NeptunePlus MC-ICP-MS in the Isotope Geology and Geochemistry department at the University of Göttingen. The introduction system consisted in a Cetac Aridus III desolvator and a Savillex PFA nebuliser (~70 µL/min uptake rate). The Mo isotopes used in the double spike deconvolution, *i.e.* ^{95}Mo, ^{97}Mo, ^{98}Mo and ^{100}Mo, were measured together with ^{101}Ru and ^{99}Ru using Faraday cups equipped with 10^{11} Ω (Mo isotopes) and 10^{13}Ω (Ru isotopes) feedback resistors amplifiers. Every sample measurement was bracketed by analyses of a spiked NIST SRM3134 standard solution. Prior to each sample or standard solution measurement, an on-peak baseline measurement on a blank 0.4 M HNO_3-0.05 M HF solution was done (15 integrations of 4 s). Sample/standard solutions were measured at concentrations of ~70 ng/g (80 integrations of 4 s). Each processed sample aliquot was measured twice. A Python script and the mathematical method described by Rudge *et al*. (2009) were used for the (off-line) data deconvolution including the correction for isobaric Ru interferences. Both the Mo isotopic compositions and Mo concentrations of the samples were derived from this spike inversion. Mo isotopic compositions are presented in $\delta^{98/95}$Mo notation, which represents the parts per thousand deviation from the bracketing NIST SRM 3134 measurements.

Japan Geological Survey (JGS) reference materials were prepared identically to the samples, *i.e.* stocks were prepared for each standard and were aliquoted, with each aliquot measured twice (like for the samples). This yielded isotopic compositions of +0.03 ± 0.05 ‰ (2 s.d.) for JB-2 (n = 5), −0.17 ± 0.03 ‰ (2 s.d.) for AGV-2 (n = 8) and −0.04 ± 0.01 ‰ (2 s.d.) for JR-2 (n = 3). These values are identical within uncertainties to previously published averages if available (JB-2 and AGV-2; *e.g.*, in Freymuth *et al*., 2015; Villalobos-Orchard *et al*., 2020; Ahmad *et al*., 2021). Based on the 2 s.d. of processed JGS reference materials, the reproducibility of our Mo isotope analyses is ±0.5 ‰. Total procedural blanks ranged between 40 and 220 pg, which amounts to less than 0.8 % of the Mo from the samples. Blank-

corrected and uncorrected $\delta^{98/95}$Mo values are identical within uncertainties, and the latter are presented in the manuscript. Mo concentrations for JB-2, AGV-2 and JR-2 (obtained from the deconvolution) were 913 ± 102 ng/g (2 s.d.), 1870 ± 80 ng/g and 2642 ± 43 ng/g, respectively, which again, are well within the range of published values when available (JB-2 and AGV-2; *e.g.*, Villalobos-Orchard *et al*., 2020).

Details for Modelled Impact of Fluid Exsolution in Discussion

The modelling discussed in the section 'Implications for the Composition of the Upper Continental Crust' uses the equation that governs isotopic fractionation in a Rayleigh distillation process:

$$(\delta^{98/95}\text{Mo})_{\text{melt}} = [(\delta^{98/95}\text{Mo})_{\text{initial melt}} + 1000]f^{(\alpha - 1)} - 1000 \quad \text{(S-1)}$$

where $\delta^{98/95}\text{Mo}_{\text{melt}}$ is the $\delta^{98/95}$Mo of the melt after fluid exsolution, $\delta^{98/95}\text{Mo}_{\text{initial melt}}$ is the $\delta^{98/95}$Mo of the initial melt, which is set to 0 ‰ in our calculation and α is the fractionation factor, defined as:

$$\alpha = (^{98}\text{Mo}/^{95}\text{Mo})_{\text{fluid}} / (^{98}\text{Mo}/^{95}\text{Mo})_{\text{melt}} \quad \text{(S-2)}$$

but set to 0.9995 in our calculation, which corresponds to a $\Delta^{98/95}\text{Mo}_{\text{fluid-melt}}$ (‰) = −0.51 ‰ (extrapolated value at ASI = 1.25 based on linear regression; see text for explanation).

The fraction of Mo remaining in the melt (*f*) is calculated as:

$$f = F \times C_{\text{Mo,melt}}/C_{\text{Mo,initial melt}} \quad \text{(S-3)}$$

where *F* is the fraction of melt remaining and is set at 0.9 to model the extraction of 10 % fluid. $C_{\text{Mo,initial melt}}$ is the Mo concentration in the initial melt and is set to 1 µg/g in our calculation and $C_{\text{Mo,melt}}$ is the Mo concentration in the remaining melt, calculated as:

$$C_{\text{Mo,melt}} = C_{\text{Mo,initial melt}} \times F^{(D_{\text{fluid-melt}}-1)} \quad \text{(S-4)}$$

where $D_{\text{fluid-melt}}$ is the Mo partition coefficient between fluid and melt, here set to 0.6, which is the maximum value obtained in our experiments.

Results of the calculations and key parameters are shown in Table S-1.

Supplementary Table

Table S-1 Calculations of the Mo isotopic composition of a melt after 10 % fluid exsolution.

	Initial melt	Magma after 10 % fluid exsolution
f (fraction of Mo remaining)	1	0.94
F (fraction of melt remaining)	1	0.90
C_{Mo} (µg/g)	1	1.04
$\delta^{98/95}Mo_{melt}$	0	0.03

Supplementary Information References

Ahmad, Q., Wille, M., König, S., Rosca, C., Hensel, A., Pettke, T., Hermann, J. (2021) The Molybdenum isotope subduction recycling conundrum: A case study from the Tongan subduction zone, Western Alps and Alpine Corsica. *Chemical Geology* 576, 120231. https://doi.org/10.1016/j.chemgeo.2021.120231

Andújar, J., Costa, F., Scaillet, B. (2013) Storage conditions and eruptive dynamics of central versus flank eruptions in volcanic islands: The case of Tenerife (Canary Islands, Spain). *Journal of Volcanology and Geothermal Research* 260, 62–79. https://doi.org/10.1016/j.jvolgeores.2013.05.004

Freymuth, H., Vils, F., Willbold, M., Taylor, R.N., Elliott, T. (2015) Molybdenum mobility and isotopic fractionation during subduction at the Mariana arc. *Earth and Planetary Science Letters* 432, 176–186. https://doi.org/10.1016/j.epsl.2015.10.006

Gaillard, F., Scaillet, B., Pichavant, M., Bény, J.-M. (2001) The effect of water and fO_2 on the ferric–ferrous ratio of silicic melts. *Chemical Geology* 174, 255–273. https://doi.org/10.1016/S0009-2541(00)00319-3

Guo, H., Li, W.-Y., Nan, X., Huang, F. (2020a) Experimental evidence for light Ba isotopes favouring aqueous fluids over silicate melts. *Geochemical Perspectives Letters* 16, 6–11. https://doi.org/10.7185/geochemlet.2036

Guo, H., Xia, Y., Bai, R., Zhang, X., Huang, F. (2020b) Experiments on Cu-isotope fractionation between chlorine-bearing fluid and silicate magma: implications for fluid exsolution and porphyry Cu deposits. *National Science Review* 7, 1319–1330. https://doi.org/10.1093/nsr/nwz221

Guo, H., Xia, Y., Wu, F., Huang, F. (2021) Zinc isotopic fractionation between aqueous fluids and silicate magmas: An experimental study. *Geochimica et Cosmochimica Acta* 311, 226–237. https://doi.org/10.1016/j.gca.2021.06.028

Keppler, H. (2010) The distribution of sulfur between haplogranitic melts and aqueous fluids. *Geochimica et Cosmochimica Acta* 74, 645–660. https://doi.org/10.1016/j.gca.2009.10.010

Keppler, H., Wyllie, P.J. (1991) Partitioning of Cu, Sn, Mo, W, U, and Th between melt and aqueous fluid in the systems haplogranite-H_2O−HCl and haplogranite-H_2O−HF. *Contributions to Mineralogy and Petrology* 109, 139–150. https://doi.org/10.1007/BF00306474

Matthews, W., Linnen, R.L., Guo, Q. (2003) A filler-rod technique for controlling redox conditions in cold-seal pressure vessels. *American Mineralogist* 88, 701–707. https://doi.org/10.2138/am-2003-0424

Rudge, J.F., Reynolds, B.C., Bourdon, B. (2009) The double spike toolbox. *Chemical Geology* 265, 420–431. https://doi.org/10.1016/j.chemgeo.2009.05.010

Villalobos-Orchard, J., Freymuth, H., O'Driscoll, B., Elliott, T., Williams, H., Casalini, M., Willbold, M. (2020) Molybdenum isotope ratios in Izu arc basalts: The control of subduction zone fluids on compositional variations in arc volcanic systems. *Geochimica et Cosmochimica Acta* 288, 68–82. https://doi.org/10.1016/j.gca.2020.07.043

Willbold, M., Hibbert, K., Lai, Y.-J., Freymuth, H., Hin, R.C., Coath, C., Vils, F., Elliott, T. (2016) High-Precision Mass-Dependent Molybdenum Isotope Variations in Magmatic Rocks Determined by Double-Spike MC-ICP-MS. *Geostandards and Geoanalytical Research* 40, 389–403. https://doi.org/10.1111/j.1751-908X.2015.00388.x